Materials Science-Poland, *Vol. 27*, *No. 2*, *2009*

Dielectric relaxation and ac conductivity of WO_3 added $(Na_{1/2}Bi_{1/2})TiO_3$ ceramic

K. PRASAD[1*], K. KUMARI[1], K. P. CHANDRA[2], K. L. YADAV[3], S. SEN[4]

[1]Materials Research Laboratory, University Department of Physics, T. M. Bhagalpur University, Bhagalpur 812 007, India

[2]Department of Physics, S.M. College, T. M. Bhagalpur University, Bhagalpur 812 001, India

[3]Department of Physics, Indian Institute of Technology, Roorkee 247 667, India

[4]National Metallurgical Laboratory, Jamshedpur 831 007, India

Ceramic samples of WO_3 added $(Na_{1/2}Bi_{1/2})TiO_3$ were prepared using a high-temperature solid-state reaction method. X-ray diffraction analyses indicate the formation of a single-phase orthorhombic structure. The apparent particle size and lattice strain are estimated using the Williamson–Hall plot. Dielectric studies revealed the relaxor behaviour and addition of WO_3 shifted phase transition temperature as well as depolarization temperature of $(Na_{1/2}Bi_{1/2})TiO_3$ to higher side. ac impedance plots were used to analyse the electrical behaviour of samples in function of frequency at various temperatures. The ac impedance studies revealed the presence of the grain boundary effect and evidence of a negative temperature coefficient of resistance. Cole–Cole analysis indicated a non-Debye type dielectric relaxation. The ac conductivity obeys the universal power law. The pair approximation type correlated barrier hopping model explains the universal behaviour of the *s* exponent. The apparent activation energy of the conduction process and density of states at the Fermi level have been discussed.

Key words: *$(Na_{1/2}Bi_{1/2})TiO_3$; impedance spectroscopy; dielectric relaxation; ac conductivity*

1. Introduction

In recent years, a number of perovskite ABO_3-type lead-free materials have been studied for their possible use in electronic applications. To date, lead-based compounds such as $Pb(Zr,Ti)O_3$, $PbTiO_3$, $Pb(Mg_{1/3}Nb_{2/3})O_3$, etc. have been widely used for multilayer capacitor, pyroelectric and/or piezoelectric applications. However, a need of lead-free materials has been felt worldwide for environmental protection. Recently, the legislation on waste electrical/electronic equipment (WEEE) and a re-

[*]Corresponding author, e-mail: k.prasad65@gmail.com; k_prasad65@yahoo.co.in

striction of hazardous substances (RoHS) has been issued by the European Union. The use of hazardous substances such as lead in electrical parts has been prohibited since 2006. To meet this requirement, the search for alternative environment-friendly lead-free materials for these applications has become the current trend. Sodium bismuth titanate, $(Na_{1/2}Bi_{1/2})TiO_3$ (NBT) is considered to be an excellent candidate as a key material of lead-free piezoelectric ceramic, which shows strong ferroelectric properties [1–7]. NBT belongs to perovskite family with rhombohedral symmetry at ambient temperature having a Curie temperature, T_m = 320 °C, and large remanent polarization, P_r = 38 μC/cm^2.

Furthermore, it has been reported that the NBT-based composition modified with $BaTiO_3$ [8,9], $Ba(Zr,Ti)O_3$ [10], $Ba(Cu_{1/2}W_{1/2})O_3$ [11], $SrTiO_3$ [12], $NaNbO_3$ [13], $MnCO_3$ [14], La_2O_3 [15,16], CeO_2 [16,17], Bi_2O_3-Sc_2O_3 [18], $LiTaO_3$ [19], ZrO_2 [20], etc. showed improved electrical as well as electromechanical properties. In addition, NBT exhibits an anomaly in its dielectric properties as a result of low temperature phase transition from a ferroelectric to an antiferroelectric phase at about 200 °C, which is termed the depolarization temperature T_d. Thus T_d is an important factor in NBT and NBT-based ceramics, in view of their practical uses, because the piezoelectric response disappears above T_d. It has also been seen that additives such as $SrTiO_3$, $BaTiO_3$, $(K_{1/2}Bi_{1/2})TiO_3$, etc. show better piezoelectric properties while the T_d is greatly reduced [11, 21]. Besides, it has been found that the addition of WO_3 improves the electrical properties of a similar perovskite system [22, 23]. A recent study on dielectric properties of the 2.5 wt. % WO_3 added $(Na_{1/2}Bi_{1/2})TiO_3$ system showed a remarkable shift in T_m as well as T_d to higher values [24].

Accordingly, in the present work, structural, microstructural, dielectric and impedance studies of 2.5 wt. % WO_3 added $(Na_{1/2}Bi_{1/2})TiO_3$ (abbreviated hereafter NBT -WO_3) ceramic are presented. An attempt has also been made to understand the mechanism of charge transport and the role of grain and grain boundaries on the electrical properties of NBT-WO_3 using complex impedance spectroscopy. The apparent activation energy of the conduction process and density of states at the Fermi level in the system are also evaluated.

2. Experimental

Polycrystalline samples of 2.5 wt. % WO_3 added $(Na_{1/2}Bi_{1/2})TiO_3$ were obtained from AR-grade (99.9%, pure) chemicals (Na_2CO_3, Bi_2O_3, TiO_2 and WO_3) using the solid-state reaction technique. The details of the sample preparation conditions have been discussed elsewhere [24]. The calcination and sintering conditions were kept at 1050 °C for 4 h and 1090 °C for 3 h, respectively. Completion of the reaction and the formation of the desired compound were checked by X-ray diffraction method. The weight of the sample was monitored before and after heat treatments. The maximum difference was about 1.12 mg for the total 10 g of the sample. Therefore, the composi-

tion of the sample was considered to be the same as the initial one. The XRD data were collected on calcined powder with an X-ray diffractometer (Siemens D500) at room temperature, using CoK_α radiation (λ = 1.7902 Å), over a wide range of Bragg angles ($20° \le 2\theta \le 80°$) with the scanning rate of 2 deg·min^{-1}. The microstructure of the sintered NBT-WO_3 sample was taken on the fractured surface using a computer controlled scanning electron microscope (JEOL-JSM840A). The frequency dependent electric permittivity (ε), electrical impedance (Z), phase angle (θ) and loss tangent ($\tan\delta$) were measured at various temperatures using a computer-controlled LCR Hi-Tester (HIOKI 3532-50), Japan, on a symmetrical cell of type Ag|ceramic|Ag, where Ag is a conductive paint coated on either side of the pellet. ac conductivity data were obtained from impedance data, using the relation $\sigma_{ac} = t/(SZ')$, where Z' is the real part of impedance, t and S are the thickness and area of the sample, respectively.

3. Results and discussion

Figure 1 shows the X-ray diffraction (XRD) profile of NBT-WO_3 at room temperature. A standard computer program, 'PowdMult' [25], was utilized for the XRD profile analysis. A good agreement between the observed and calculated interplane spacing and no trace of any extra peaks due to constituent oxides were found, thereby suggesting the formation of a single-phase compound having an orthorhombic structure.

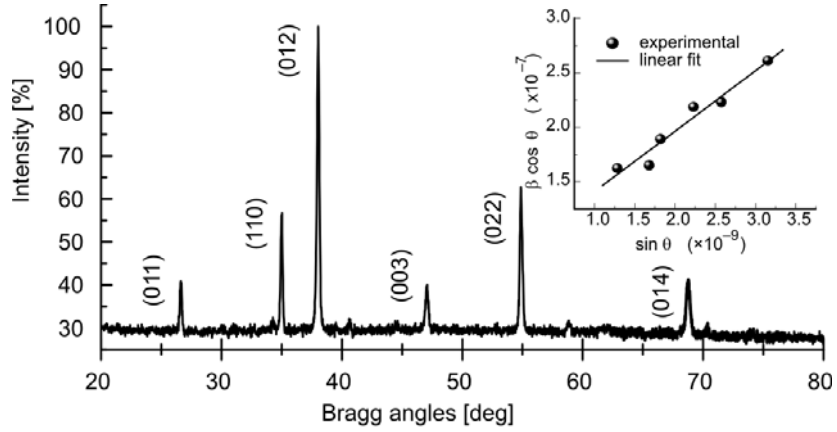

Fig. 1. Indexed X-ray diffraction pattern of NBT WO_3 at room temperature. Inset: the Williamson–Hall plot

The lattice parameters were found to be: a = 3.808(8) Å, b = 4.764(4) Å and c = 6.722(2) Å, with an estimated error of $\pm 10^{-3}$ Å. The unit cell volume was estimated to be 121.99 Å^3. The apparent particle size and lattice strain of NBT-WO_3 were estimated by analyzing the X-ray diffraction peak broadening, using the Williamson–Hall approach [26]:

$$\beta\cos\theta = 2\frac{\Delta\xi}{\xi}\sin\theta + \frac{K\lambda}{D} \tag{1}$$

where D is the apparent particle size, β is the diffraction peak width at half intensity (FWHM) and $\Delta\xi/\xi$ is the lattice strain and K is the Scherrer constant (0.89). The term $K\lambda/D$ represents the Scherrer particle size distribution. The lattice strain can be estimated from the slope of the plot $\beta\cos\theta$ in function of $\sin\theta$, and the apparent particle size can be estimated from the intersection of this line at $\sin\theta = 0$. Linear least squares fitting to $\beta\cos\theta/\lambda - \sin\theta/\lambda$ data provided the values of the intercept and slope of the plot. A Gaussian model was applied to estimate the diffraction peak width at a half intensity.

$$I = I_0 + \frac{A}{\beta\sqrt{\frac{\pi}{2}}}\exp\left(-2\left(\frac{\theta-\theta_c}{\beta}\right)^2\right) \tag{2}$$

where A and θ_c are the area and centre of the curve, respectively. The inset of Fig. 1 illustrates the Williamson–Hall plot for NBT-WO_3. The apparent particle size and lattice strain are estimated, respectively, to be of the order of 104 nm and 0.0056.

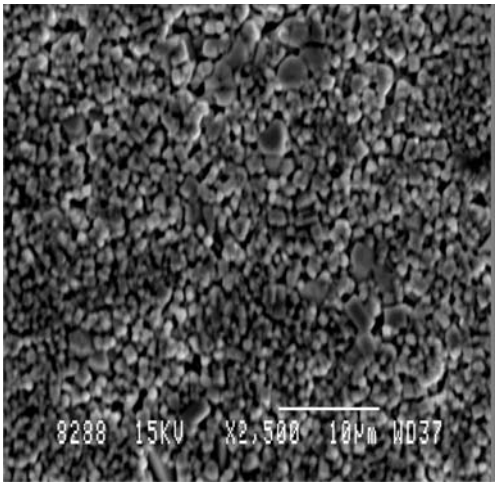

Fig. 2. SEM micrograph of NBT-WO_3 at 10 μm magnification

Figure 2 shows the SEM micrograph of NBT-WO_3 at 10 μm magnification. Grain shapes are clearly visible, indicating the existence of polycrystalline microstructure. Grains of unequal sizes appear to be distributed throughout the sample. The average grain size was estimated to be about 2.5 μm. The ratio of the grain size to apparent particle size of NBT-WO_3 is found to be of the order of 24.

Figure 3 presents the temperature dependences of ε and $\tan\delta$ at three representative frequencies for NBT-WO_3 system. It can be seen that the temperature of maximum relative permittivity (T_m) shifted to a higher temperature (from 440 °C at 1 kHz

to 465 °C at 100 kHz) and ε_m decreased from 3139 at 1 kHz to 1001 at 100 kHz with the increase in frequency. Also, the plots show the diffuse phase transition (DPT) around 10 °C and a strong frequency dispersion, which indicates the relaxor behavior in NBT-WO_3. Besides, it is important to note that the addition of WO_3 to NBT shifts T_m as well as T_d to higher temperature by more than 100 °C which is desirable for piezoelectric applications. The room temperature value of ε and tanδ at 1 kHz were found to be 424 and 0.18, respectively.

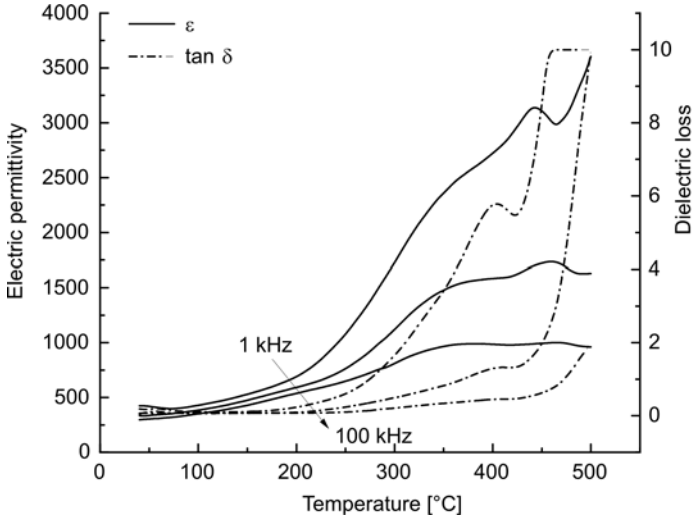

Fig. 3. Temperature dependences of ε and tanδ of NBT-WO_3 at 1, 10 and 100 kHz

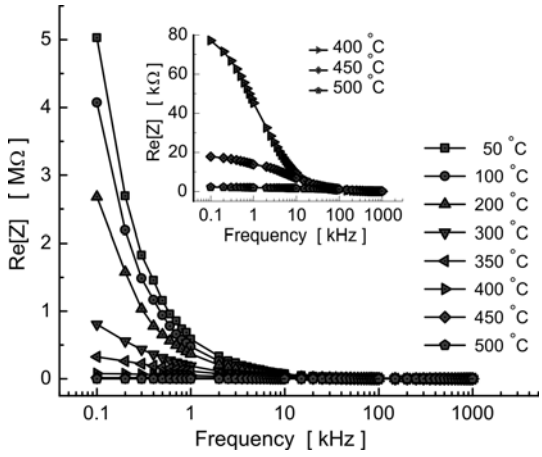

Fig. 4. Dependences of the real part of impedance of NBT-WO_3 on frequency at various temperatures. The inset shows an enlarged view at 400 °C, 450 °C and 500 °C

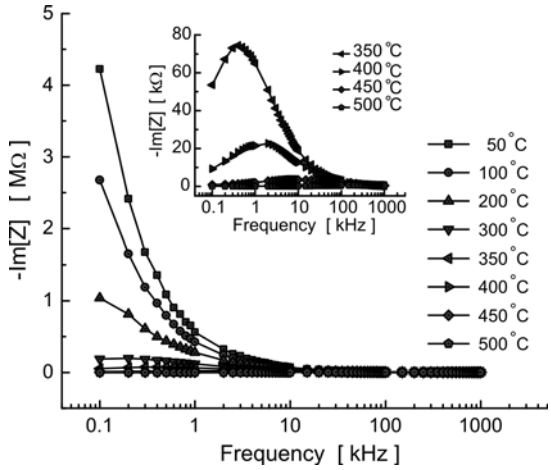

Fig. 5. Dependences of the imaginary part of impedance of NBT-WO_3 on frequency at various temperatures. The inset shows an enlarged view at 350–500 °C

Figures 4, 5 and their insets show the dependences of the real (Z') and imaginary (Z'') parts of impedance on frequency at various temperatures. The value of Z' decreases with increasing temperature as well as with increasing frequency which shows that NBT-WO_3 has the negative temperature coefficient of resistance (NTCR). This indicates an increase in the ac conductivity with the increase in temperature and frequency. The loss spectrum (Fig. 5) is characterized by some important features in the pattern such as the appearance of a peak ($Z''_{\max}$), asymmetric peak broadening (inset of Fig. 5) and the decrease of values of $Z''_{\max}$ which shift to higher temperatures with the increasing frequency. The asymmetric broadening of peaks in frequency explicit plots of Z'' suggests that there is a spread of relaxation times, i.e. the existence of a temperature dependent electrical relaxation phenomenon in the material.

Figure 6 shows the complex impedance plots at various temperatures in a logarithmic scale. It is observed that the impedance data at room temperature do not take the shape of a semicircle but rather resemble a straight line, suggesting the insulating behaviour of NBT-WO_3. It can also be seen that with the increase in temperature the slope of the lines decreases, and the lines bend towards the real (Z') axis. Also, at 300 °C a single semicircle, and at 400 °C and above two semicircles could be obtained with different values of resistance for grain (R_b) and grain boundary (R_{gb}). This indicates the increase in conductivity of the sample with the increase of temperature. Hence, the grain and grain boundary effects could be separated at these temperatures. It can also be observed that the peak maxima of the plots decrease and the frequency for the maximum shifts to higher values with the increase in temperature. Furthermore, it can be seen that the Cole–Cole plots (inset of Fig. 6) are not represented by a full semicircle, and the centre of the arc lies below the real (Z') axis, which suggests that the dielectric relaxation is of non-Debye type in NBT-WO_3. This may be due to the presence of distributed elements in the material-electrode system [27].

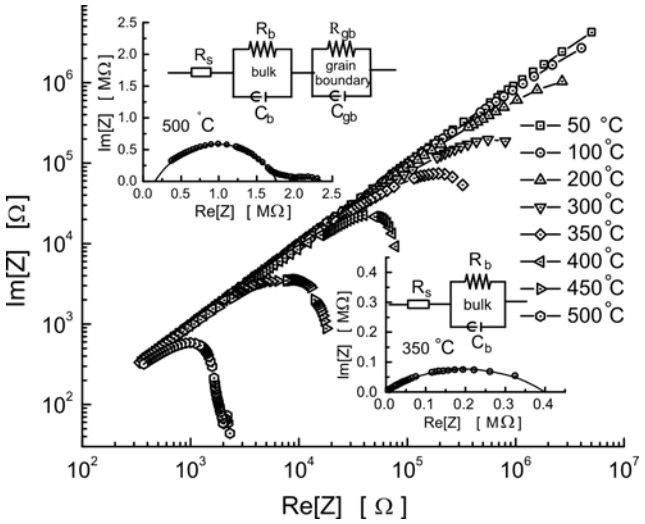

Fig. 6. Complex impedance plots of NBT-WO_3 at various temperatures in a logarithmic scale. The inset shows the Cole–Cole plots at 350 °C and 500 °C with the appropriate, equivalent electrical circuit

It is believed that the correlation among the Debye relaxators may start developing via formation of nanopolar clusters of Na-TiO_3 and Bi-TiO_3. Since the relaxation times of the relaxators within polar clusters are distributed over a wide spectrum at higher temperatures, their responses to an external field are in a different time domain. This results in the deviation from the Cole–Cole plots [28–30]. The first semicircle (which may be ascribed to a parallel combination of bulk resistance R_b and capacitance C_b), in a high frequency region corresponds to the intragranular behaviour of the material or bulk properties. The second semicircle (which may be attributed to a parallel combination of grain boundary resistance, R_{gb} and capacitance, C_{gb}), in a low frequency region represents the grain boundary contribution. It is obvious that the conductivities of grains and grain boundaries may be different, owing to different underlying processes, and thereby relax in different frequency regions. In such a case, the equivalent circuits (inset of Fig. 6) can be represented as a series network of parallel *RC* elements [27]. The impedance can then be expressed as:

$$Z^* = (R_b^{-1} + j\omega C_b)^{-1} + (R_{gb}^{-1} + j\omega C_{gb})^{-1} \tag{3}$$

The values of R_b and R_{gb} could directly be obtained from the intercept of the ends of the semicircle on the Z' axis whose temperature dependences are shown in Fig. 7. It can be seen that the values of R_b and R_{gb} decrease with the increase of temperature, which clearly indicates the NTCR character of NBT-WO_3 and supports Fig.4. The capacitances (C_b and C_{gb}) due to these effects can be estimated using the relation:

$$\omega_{\max} RC = 1 \tag{4}$$

where ω_{max} (= $2\pi f_{max}$) is the angular frequency at the maximum of the semicircle. Figure 7 shows the temperature dependences of C_b and C_{gb} obtained from the Cole–Cole plots at various temperatures. The decrease in the value of R_b of NBT-WO_3 is associated with an increase in conductivity with the increase in temperature. Also, a decrease in the R_{gb} values with the increment of temperature suggests the lowering of the barrier towards the mobility of charge carriers aiding electrical conduction at higher temperatures [30]. Besides, these curves do not coincide with the origin; rather they start from ~350 Ω. Therefore, a series resistance R_s =350 Ω should be added to the LCR circuit representation (inset of Fig. 6) of the sample.

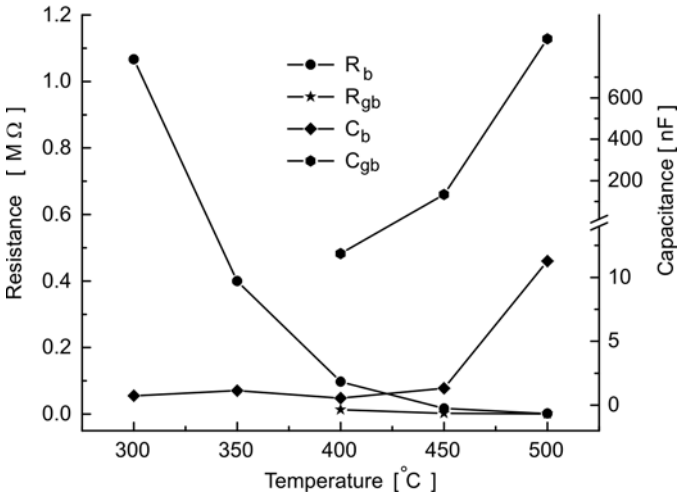

Fig. 7. Temperature dependences of R_b, R_{gb}, C_b and C_{gb} of NBT-WO_3

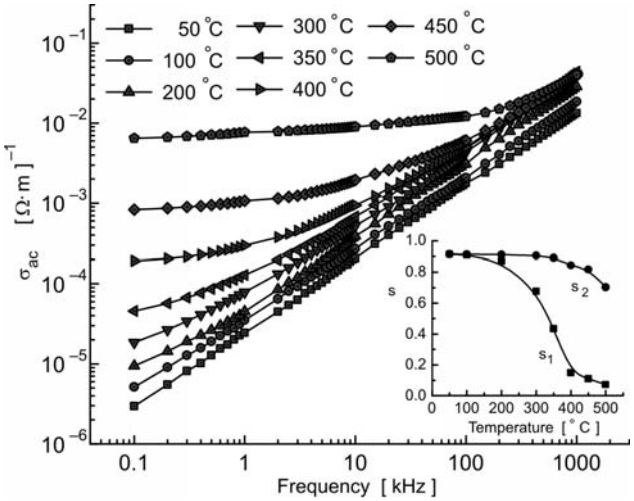

Fig. 8. Dependences of ac conductivity on frequency at various temperatures of NBT-WO_3. Inset: Temperature dependence of index s

Figure 8 shows the log–log dependences of electrical conductivity on frequency at various temperatures. The pattern of the conductivity spectrum shows dispersion throughout the chosen frequency range. The frequency dependence of the ac conductivity at room temperature obeys the universal power law [31]:

$$\sigma_{ac} = A\omega^S \tag{5}$$

whereas above room temperature this dependence follows the double power law of type [32]:

$$\sigma_{ac} = A_1\omega^{S_1} + A_2\omega^{S_2} \tag{6}$$

where A, A_1 and A_2 are the temperature dependent constants, and s, s_1 and s_2 are the temperature as well as frequency dependent parameters. Such dependence is associated with displacement of carriers which move within the sample by discrete hops of the length R between randomly distributed, localized sites. The values of the indices s_1 and s_2 can be obtained from the slopes in the low and high frequency regions, respectively. The inset of Fig. 8 shows the temperature dependences of s_1 and s_2. It can be seen that the values of both s_1 and s_2 are always lower than 1, and decrease with the increase of temperature. Furthermore, the value of s_1 approaches zero at higher temperatures, indicating that dc conductivity dominates at higher temperatures in the low frequency region and obeys Jonscher's power law [33]:

$$\sigma_{ac} = \sigma(0) + A\omega^{S_2} \tag{7}$$

where $\sigma(0)$ is the frequency independent part of the conductivity. The model based on correlated hopping of electrons over a barrier [34] predicts a decrease in the value of the index with the increase in temperature, and it was found to be consistent with the experimental results. Therefore, the electrical conduction in the system could be considered due to the short-range translational type hopping of charge carriers [30, 32, 35]. This indicates that the conduction process is thermally activated. The exponent s_i (i = 1 or 2) and binding energies are related by:

$$s_i = 1 - \frac{6k_BT}{W_m} \tag{8}$$

A decrease of W_m upon temperature increase was observed. The characteristic decrease in slopes (s_1 and s_2) with the increase of temperature is due to the decrease in binding energy [35].

Figure 9 shows the dependence of ac conductivity on T^{-1}. A linear least squares fit of $\ln\sigma_{ac}$–$10^3/T$ data in the higher temperature region gives the value of the apparent activation energy of the conduction process. It has been observed that the value of the activation energy (0.019 eV at 1 kHz) decreases with the increase in frequency. It can be seen that the ac conductivity is almost insensitive in the low temperature region, irrespective of the operating frequencies. Also, the onset temperature shifts to a higher

temperature with the increase in frequency. A low value of the activation energy obtained could be attributed to the influence of an electronic contribution to the conductivity in which the transport of carriers may occur through hopping between localized states in a disordered manner. Also, the increase in conductivity with temperature may be explained based on the assumption that within the bulk, the oxygen vacancies, due to the loss of oxygen, are usually created during sintering and the charge compensation, which may leave behind free electrons, making them n-type.

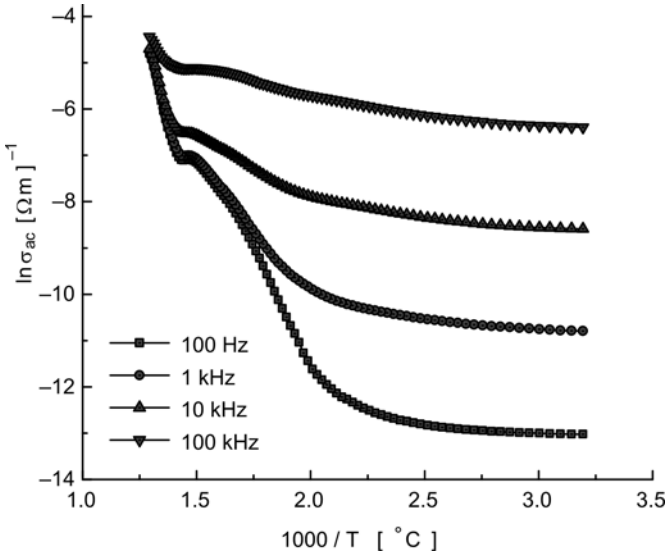

Fig. 9. Dependence of ac conductivity of NBT-WO_3on inverse of temperature at various frequencies

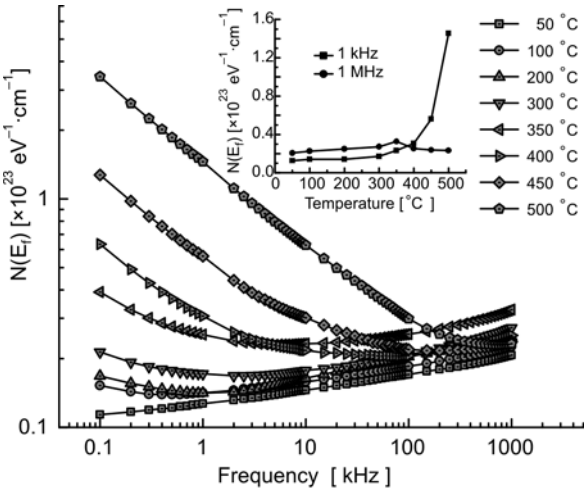

Fig. 10. Frequency dependence of $N(E_f)$ in NBT-WO_3 at various temperatures.
Inset: Temperature dependences of $N(E_f)$ at 1 kHz and 1 MHz

The hopping conduction mechanism is generally consistent with the existence of a high density of states in the materials having a band gap similar to that of a semiconductor. Due to localization of charge carriers, formation of polarons takes place and the hopping conduction may occur between the nearest neighbouring sites. The ac conductivity data were used to evaluate the density of states at the Fermi level $N(E_f)$ using the dependence [36]:

$$\sigma_{ac}(\omega) = \frac{\pi}{3} e^2 \omega k_B T \left(N(E_f) \right)^2 \alpha^{-5} \left(\ln \frac{f_0}{\omega} \right)^4 \tag{9}$$

where e is the electronic charge, f_0 the photon frequency and α is the localized wave function, assuming $f_0 = 10^{13}$ Hz, $\alpha = 10^{10}$ m^{-1} at various operating frequencies and temperatures. Figure 10 shows the frequency dependence of $N(E_f)$ at different temperatures. As can be seen the value of $N(E_f)$ increases with the increase in operating frequency at low temperatures showing a minimum (from 100 °C onwards) which shift towards higher frequencies with the increasing temperature. The inset of Fig. 10 shows the variation of $N(E_f)$ with temperature at two representative frequencies: 1 kHz and 1 MHz. It is found that the value of $N(E_f)$ increases with the increase in temperature at low frequencies, while it shows a maximum at 350 °C at 1 MHz. The reasonably high values of $N(E_f)$ suggest that the hopping between the pairs of sites dominate the mechanism of charge transport in NBT-WO_3.

4. Conclusion

Polycrystalline samples of 2.5 wt. % WO_3 added $(Na_{1/2}Bi_{1/2})TiO_3$, prepared by a high-temperature solid-state reaction technique, were found to have a single-phase perovskite-type orthorhombic structure. Impedance analyses indicated the presence of grain and grain boundary effects. The dielectric relaxation in the system was found to be of non-Debye type. The ac conductivity was found to obey the universal power law. The pair approximation type correlated barrier hopping (CBH) model accurately describes the mechanism of charge transport in NBT-WO_3 system.

References

[1] GOMAH-PETTRY J.R., SAÏD S., MARCHET P., MERCURIO J.P., J. Eur. Ceram. Soc., 24 (2004), 1165.
[2] XU Q., CHEN S., CHEN W., WU S., ZHOU J., SUN H., LI Y., Mater. Chem. Phys., 90 (2005), 111.
[3] BUHRER C.F., J. Chem. Phys., 36 (1962), 798.
[4] SUCHANICZ J., ROLEDER K., KANIA A., HANDEREK J., Ferroelectrics, 77 (1988), 107.
[5] ROHLEDER K., SUCHANICZ J., KANIA A., Ferroelectrics, 89 (1989), 1.
[6] HOSONO Y., HARADA K., YAMASHITA Y., Jpn. J. Appl. Phys., 40 (2001), 5722.
[7] SUCHANICZ J., KUSZ J., BHÖM H., DUDA H., MERCURIO J.P., KONIECZNY K., J. Eur. Ceram. Soc., 23 (2003), 1559.
[8] TAKEDA H., AOTO W., SHIOSAKI T., Appl. Phys. Lett., 87 (2005), 102104.

[9] WANG X.X., TANG X.G., CHAN H.L.W., Appl. Phys. Lett., 85 (2004), 91.
[10] PENG C., LI J-F., GONG W., Mater. Lett., 59 (2005), 1576.
[11] CHU B.J., CHEN D.R., LI G.R., YIN Q.R., J. Eur. Ceram. Soc., 22 (2002), 2115.
[12] GUO Y., KAKIMOTO KEN-ICHI, OHSATO H., Solid State Commun., 129 (2004), 279.
[13] LI Y.M., CHEN W., ZHOU J., XU Q., GU X.Y., LIAO R.H., Physica B, 365 (2005), 76.
[14] NAGATA H., TAKENAKA T., J. Eur. Ceram. Soc. 21 (2001), 1299.
[15] HERABUT A., SAFARI A., J. Amer. Ceram. Soc. 80 (1997), 2954.
[16] WANG X.X., CHAN H.L.W., CHOY C.L., Appl. Phys. A 80 (2005), 333.
[17] LI Y., CHEN W., XU Q., ZHOU J., WANG Y., SUN H., Ceram. Int., 33 (2007), 95.
[18] TAKENAKA T., NAGATA H., Jpn. J. Appl. Phys., 30 (1991), 2236.
[19] GUO Y., KAKIMOTO K-I., OHSATO H., Mater. Lett., 59 (2005), 241.
[20] LILY, KUMARI K., PRASAD K., CHOUDHARY R.N.P., J. Alloys Comp., 453 (2008), 325.
[21] ZHAO S., LI G., DING A., WANG T., YIN Q., J. Phys. D: Appl. Phys., 39 (2006), 2277.
[22] UEDA I., Jpn. J. Appl. Phys., 11 (1972), 450.
[23] ZHONG N., DONG X., SUN D., DU H., YANG H., Mater. Sci. Eng. B, 106 (2004), 263.
[24] PRASAD K., KUMARI K., LILY, CHANDRA K.P., YADAV K.L., SEN S., Solid State Commun., 144 (2007), 42.
[25] *PowdMult*, *An interactive powder diffraction data interpretation and indexing program*, ver. 2.1, School of Physical Science, Flinders University of South Australia, Bedford Park, S. A. 5042, Australia.
[26] SURYANARAYANA C., GRANT NORTON M., *X-Ray Diffraction A Practical Approach*, Plenum Press, New York, 1998.
[27] *Impedance Spectroscopy Emphasizing Solid Materials and Systems*, J.R. Macdonald (Ed.), Wiley, New York, 1987.
[28] BONNEAU P., GARNIER O., CALVARIN G., HUSSON E., GAVARRI J.R., HEWAT A.W., MORREL A., J. Solid State Chem., 91 (1991), 350.
[29] LILY, KUMARI K., PRASAD K., YADAV K.L., J. Mater. Sci., 42 (2007), 6252.
[30] PRASAD K., LILY, KUMARI K., CHANDRA K.P., YADAV K.L., SEN S., Appl. Phys. A., 88 (2007), 377.
[31] MOTT N.F., DAVIS E.A., *Electronic Processes in Non-Crystalline Materials*, Oxford University Press, London, 1979.
[32] FUNKE K., Prog. Solid State Chem., 22 (1993), 111.
[33] JONSCHER A.K., Nature, 267 (1977), 673.
[34] ELLIOTT S.R., Philos. Mag. B, 37 (1978), 553.
[35] PRASAD K., KUMARI K., LILY, CHANDRA K.P., YADAV K.L., SEN S., Adv. Appl. Ceram., 106 (2007), 241.
[36] SHARMA G.D., ROY M., ROY M.S., Mater. Sci. Eng. B, 104 (2003), 15.

Received 19 June 2008